Advances in Water Resources 115 (2018) 172–184

Contents lists available at ScienceDirect

Advances in Water Resources

journal homepage: www.elsevier.com/locate/advwatres

Positivity-preserving well-balanced discontinuous Galerkin methods for the shallow water flows in open channels

Shouguo Qian[a], Gang Li[a], Fengjing Shao[b], Yulong Xing[c,*]

[a] School of Mathematics and Statistics, Qingdao University, Qingdao, Shandong 266071, PR China
[b] Institute of Complexity Science, Qingdao University, Qingdao, Shandong 266071, PR China
[c] Department of Mathematics, Ohio State University, Columbus, OH 43210, USA

ARTICLE INFO

Article history:
Received 11 December 2017
Revised 28 February 2018
Accepted 1 March 2018
Available online 8 March 2018

Keywords:
Shallow water flows
Cross section
Discontinuous Galerkin
Well-balanced
Positivity-preserving method

ABSTRACT

We construct and study efficient high order discontinuous Galerkin methods for the shallow water flows in open channels with irregular geometry and a non-flat bottom topography in this paper. The proposed methods are well-balanced for the still water steady state solution, and can preserve the non-negativity of wet cross section numerically. The well-balanced property is obtained via a novel source term separation and discretization. A simple positivity-preserving limiter is employed to provide efficient and robust simulations near the wetting and drying fronts. Numerical examples are performed to verify the well-balanced property, the non-negativity of the wet cross section, and good performance for both continuous and discontinuous solutions.

© 2018 Elsevier Ltd. All rights reserved.

1. Introduction

The shallow water equations are commonly used to model and simulate flows in rivers and coastal areas. In this paper, we consider one dimensional shallow water flows in open channels with irregular geometry and a non-flat bottom topography (Hernández-Duenas and Karni, 2011; Vázquez-Céndon, 1999), taking the form of

$$H_t + Q_x = 0,$$
$$Q_t + \left(\frac{Q^2}{H} + \frac{1}{2}g\sigma h^2\right)_x = \frac{1}{2}gh^2\sigma_x - g\sigma h b_x, \tag{1}$$

where $\sigma(x)$ represents the width of the channel, b denotes the bottom topography, h is the water height, $H = \sigma h$ is the wet cross section, $Q = Hu$ is the mass flow rate, u is the velocity, and g is the gravitational constant. This model is characterized by the non-dimensional Froude number $|u|/c$ where $c = \sqrt{gH/\sigma}$, and reduces to the nonlinear shallow water equations when the cross section $\sigma(x)$ is a constant.

The shallow water flows in channels (1) belong to the class of hyperbolic equations with source terms (also referred as hyperbolic balance laws), and admit the still water steady state solution given by

$$u = 0, \qquad h + b = const, \tag{2}$$

in which the source term is exactly balanced by the flux gradient. One main challenge in the numerical simulation of such balance laws, including the nonlinear shallow water equations with a non-flat bottom topography and Euler equations under gravitation fields, is that a standard numerical method may not satisfy the balance of flux gradient and source term at the steady state in the discrete level, and may introduce spurious oscillations near the steady state. Well-balanced methods are designed to overcome this challenge, and performs well at (or near) the steady state with coarse meshes. Many well-balanced methods have been designed for the nonlinear shallow water equations, see Audusse et al. (2004), Bermudez and Vazquez (1994), Greenberg and LeRoux (1996), LeVeque (1998), Perthame and Simeoni (2001), Xu (2002), Xing (2014), Xing and Shu (2005), Xing and Shu (2013) and the references therein. Another commonly encountered challenge in the simulations of the shallow water related models is the wetting and drying treatment for the region where there is little or no water. Typical applications include the dam break problem, flood waves and run-up phenomena. Numerically, negative water may be produced during the computation, which may pose additional difficulty. There are many existing positivity-preserving techniques to overcome this difficulty, and we refer to Bokhove (2005), Bunya et al. (2009), Ern et al. (2008), Xing and Zhang (2013), Xing et al. (2010),

* Corresponding author.
E-mail address: xing.205@osu.edu (Y. Xing).

https://doi.org/10.1016/j.advwatres.2018.03.001
0309-1708/© 2018 Elsevier Ltd. All rights reserved.

Kurganov and Levy (2002) and the references therein for some recent works.

For the shallow water flows in open channels (1), an early work on well-balanced methods was carried out in 1999 by Vázquez-Céndon (1999), where the model was first reformulated into the nonlinear shallow water equations with additional source terms representing the channel width. The method proposed in Bermudez and Vazquez (1994) can then be applied to deliver well-balanced methods for the shallow water flows in channels. García-Navarro and Vázquez-Céndon (2000) designed well-balanced method using proper flux difference splitting. Recently, Balbas and Karni (2009) designed second-order well-balanced positivity-preserving numerical methods in rectangular channels using the central schemes. The extension to shallow water flows with arbitrary cross section was studied in Hernández-Duenas and Karni (2011) and Balbás and Hernández-Duenas (2014). Well-balanced method based on energy balanced property is studied in Murillo and García-Navarro (2014). Hernández-Duenas and Beljadid (2016) developed a new non-oscillatory semi-discrete central-upwind scheme coupled with artificial viscosity. Xing (2016) designed high order well-balanced finite volume weighted essentially non-oscillatory schemes for shallow water flows in open channels with irregular geometry and a non-flat bottom topography.

All of the works mentioned above for the shallow water flows in open channels are based on finite difference or finite volume schemes. During the past few decades, high order finite element discontinuous Galerkin (DG) methods have gained great attention in solving partial differential equations including the hyperbolic conservation laws. DG methods, using discontinuous piecewise polynomial space as the solution and test function spaces (see Cockburn et al., 2000 for a historic review), combine advantages of both finite element and finite volume methods, and can achieve high order of accuracy easily with the use of high order polynomials within each element. Several advantages of the DG methods, including their accuracy, high parallel efficiency, flexibility for hp-adaptivity and arbitrary geometry and meshes, make them attractive for a wide range of applications including the shallow water simulations.

The main objective of this paper is to develop efficient high order DG methods for the shallow water flows in open channels with non-flat bottom topography. The proposed methods have two attractive features: well-balanced for the still water steady state solutions and positivity-preserving near the wetting and drying front. This will be the first paper on high order DG methods for the shallow water flows in open channels to achieve these properties, to our best knowledge. To achieve well-balanced property, we start by rewriting the source terms in an equivalent special form using the still water steady state solution (2). Then we apply integration by parts on these source terms to derive a numerical approximation which is exactly well balanced with the flux gradient at the steady state and also high order accurate for general solutions. The approach to achieve high order well-balanced property is very different from the other high order method for the shallow water flows in channels presented in Xing (2016), where an extrapolation on the source term approximation was introduced to increase the order from second order to fourth order. Here we could achieve any order of accuracy in the DG framework. A simple positivity-preserving limiter, adopted from Zhang and Shu (2010) and later applied to DG methods for the shallow water equations in Xing et al. (2010), was used to ensure the resulting methods maintain the non-negativity of the cross sectional wet area.

This paper is organized as follows. In Section 2, we first present the novel high order well-balanced DG methods. The positivity-preserving technique is presented in Section 3. In Section 4, some numerical examples are presented to verify the well-balanced property, the non-negativity of the wet cross section, high order accuracy in smooth regions for general solutions and essentially non-oscillatory for general solutions with discontinuities. Finally, some conclusions are given in Section 5.

2. Well-balanced methods

In this section, we present high order well-balanced DG methods for the shallow water flows (1) in open channels, which can preserve the still water steady state (2) exactly.

2.1. Notations

We divide the interval $I = [a, b]$ into N subintervals and denote the cells by $I_j = [x_{j-\frac{1}{2}}, x_{j+\frac{1}{2}}]$ for $j = 1, \cdots, N$. The center of each cell is $x_j = \frac{1}{2}(x_{j-\frac{1}{2}} + x_{j+\frac{1}{2}})$, and the mesh size is denoted by $\tau_j = x_{j+\frac{1}{2}} - x_{j-\frac{1}{2}}$, with $\tau = \max_{1\le j\le N} \tau_j$ being the maximal mesh size. The piecewise polynomial space V_τ^k is defined as the space of polynomials of degree up to k in each cell I_j, that is,

$$V_\tau^k = \left\{ v : v|_{I_j} \in P^k(I_j),\ j = 1, 2, \cdots, N \right\}. \tag{3}$$

Note that the functions in V_τ^k are allowed to have discontinuities across element interfaces. For any unknown function v, its numerical approximation in the DG methods is denoted by v_τ, which belongs to the finite element space V_τ^k. We denote by $v^+_{\tau,j+\frac{1}{2}}$ and $v^-_{\tau,j+\frac{1}{2}}$ the limit values of v_τ at $x_{j+\frac{1}{2}}$ from the right cell I_{j+1} and from the left cell I_j, respectively. In addition, we use the usual notation, $\{v_\tau\}_{j+\frac{1}{2}} = (v^+_{\tau,j+\frac{1}{2}} + v^-_{\tau,j+\frac{1}{2}})/2$, to represent the arithmetic mean of the function v_τ at the element interface $x_{j+\frac{1}{2}}$.

2.2. Reformulation of the system and standard DG methods

The first step in designing well-balanced methods is to rewrite the source terms in an equivalent form using the information of the steady state solution (2). Here we reformulate the original governing equations as

$$\begin{aligned} &H_t + Q_x = 0, \\ &Q_t + \left(\frac{Q^2}{H} + \frac{1}{2}g\sigma h^2\right)_x = \frac{1}{2}g(h+b)^2\sigma_x - g(h+b)(\sigma b)_x \\ &\qquad\qquad + \frac{1}{2}g(\sigma b^2)_x, \end{aligned} \tag{4}$$

where we replace the source term $\frac{1}{2}gh^2\sigma_x - g\sigma h b_x$ by the equivalent form of $\frac{1}{2}g(h+b)^2\sigma_x - g(h+b)(\sigma b)_x + \frac{1}{2}g(\sigma b^2)_x$ in the momentum equation. Note that when σ is constant, this reformulation reduces to the one in Xing and Shu (2006) for the shallow water equations, therefore this can be viewed as a generalization of the technique presented in Xing and Shu (2006) for the shallow water flows in channels.

For the sake of easy presentation, we introduce the notation

$$U = \begin{pmatrix} H \\ Q \end{pmatrix}, \tag{5}$$

to denote the conservative variable, and rewrite the shallow water flows in channels (4) as

$$U_t + F(U, \sigma)_x = S(U, \sigma, \sigma b, \sigma b^2), \tag{6}$$

where $F(U, \sigma)$ and $S(U, \sigma, \sigma b, \sigma b^2)$ denote the flux and source term, respectively.

The initial condition of $U(x, 0)$ is projected into the piecewise polynomial space V_τ^k to obtain $U_\tau(x, 0)$ via the standard L^2 projection. Similarly, we project $\sigma(x)$ and $(\sigma b)(x)$ to obtain the piecewise

polynomial functions σ_τ and $(\sigma b)_\tau$. The standard DG method for the class of hyperbolic equations (6) has the form:

$$\int_{I_j} \partial_t U_\tau^n v \mathrm{d}x - \int_{I_j} F(U_\tau^n, \sigma_\tau)\partial_x v \mathrm{d}x + \widehat{F}_{j+\frac{1}{2}} v_{j+\frac{1}{2}}^- - \widehat{F}_{j-\frac{1}{2}} v_{j-\frac{1}{2}}^+ = \int_{I_j} S(U_\tau^n, \sigma_\tau, (\sigma b)_\tau, (\sigma b)_\tau^2/\sigma_\tau) v \mathrm{d}x, \tag{7}$$

with the numerical fluxes given by

$$\widehat{F}_{j+\frac{1}{2}} = f\left(U_{\tau,j+\frac{1}{2}}^{n,-}, U_{\tau,j+\frac{1}{2}}^{n,+}; \sigma_{\tau,j+\frac{1}{2}}^-, \sigma_{\tau,j+\frac{1}{2}}^+\right), \tag{8}$$

where f is a numerical flux. Herein, we adopt the simple Lax–Friedrichs flux

$$\begin{aligned} &f\left(U_{\tau,j+\frac{1}{2}}^{n,-}, U_{\tau,j+\frac{1}{2}}^{n,+}; \sigma_{\tau,j+\frac{1}{2}}^-, \sigma_{\tau,j+\frac{1}{2}}^+\right) \\ &= \frac{1}{2}\left(F\left(U_{\tau,j+\frac{1}{2}}^{n,-}, \sigma_{\tau,j+\frac{1}{2}}^-\right) + F\left(U_{\tau,j+\frac{1}{2}}^{n,+}, \sigma_{\tau,j+\frac{1}{2}}^+\right) \right. \\ &\quad \left. -\alpha\left(U_{\tau,j+\frac{1}{2}}^{n,+} - U_{\tau,j+\frac{1}{2}}^{n,-}\right)\right), \end{aligned} \tag{9}$$

where $\alpha = \max_U |\lambda(U)|$ with $\lambda(U)$ being the eigenvalues of the Jacobian $F'(U)$ and the maximum is taken over the whole region. For this system, we have $\alpha = \max_{x\in I}\left(|u_\tau| + \sqrt{gh_\tau}\right)$.

High order total variation diminishing (TVD) Runge–Kutta methods (Shu, 1988) are often used as the temporal discretization of the method (7). In the numerical examples of this paper, the third order TVD Runge–Kutta method

$$\begin{aligned} U^{(1)} &= U^n + \Delta t \mathcal{F}(U^n) \\ U^{(2)} &= \frac{3}{4}U^n + \frac{1}{4}\left(U^{(1)} + \Delta t \mathcal{F}(U^{(1)})\right) \\ U^{n+1} &= \frac{1}{3}U^n + \frac{2}{3}\left(U^{(2)} + \Delta t \mathcal{F}(U^{(2)})\right), \end{aligned} \tag{10}$$

with $\mathcal{F}(U)$ being the spatial operator, is used.

2.3. Well-balanced numerical fluxes

Note that the standard DG methods (7) presented in the preceding subsection do not have the well-balanced property. In this subsection, we present the modification to the numerical fluxes with the purpose of preserving the steady state (2) exactly.

Suppose the initial condition is given as the steady state (2), i.e., $H/\sigma + b = h + b = C$ and $Q/H = u = 0$, with C being a constant. We want to recover this steady state information using the computational variables U_τ (piecewise polynomials) at each time level. The projection of the initial condition leads to the fact that $(H_\tau + (\sigma b)_\tau)/\sigma_\tau = C$. At each time step, we introduce the functions h_τ and b_τ based on the numerical solutions as

$$h_\tau = \frac{H_\tau}{\sigma_\tau}, \qquad b_\tau = \frac{(\sigma b)_\tau}{\sigma_\tau}, \tag{11}$$

and their sum $(h+b)_\tau$ defined by:

$$(h+b)_\tau = \frac{H_\tau + (\sigma b)_\tau}{\sigma_\tau}. \tag{12}$$

Note that, inside each cell I_j, $(h+b)_\tau$ is a rational polynomial function, and may not be a polynomial. But at the steady state solution (2), we can easily obtain that $(h+b)_\tau = C$. At the cell boundary $x_{j+1/2}$, we can evaluate $U_{\tau,j+1/2}^\pm$ using the polynomials from the left and right boundaries. Similarly, we can obtain $\sigma_{\tau,j+1/2}^\pm$ and $(\sigma b)_{\tau,j+1/2}^\pm$. The cell average and cell boundary values of $(h+b)_\tau$ are defined as:

$$\overline{(h+b)}_{\tau,j} = \frac{\overline{(H_\tau + (\sigma b)_\tau)}_j}{\overline{\sigma}_{\tau,j}}, \quad (h+b)_{\tau,j+\frac{1}{2}}^\pm = \frac{H_{\tau,j+\frac{1}{2}}^\pm + (\sigma b)_{\tau,j+\frac{1}{2}}^\pm}{\sigma_{\tau,j+\frac{1}{2}}^\pm}, \tag{13}$$

which also satisfy $\overline{(h+b)}_{\tau,j} = (h+b)_{\tau,j+\frac{1}{2}}^\pm = C$ at the still water state (2). For the purpose of positivity preserving (as explained in Section 3), we also introduce the updated cell boundary values at the time step t^n as in Audusse et al. (2004)

$$h_{\tau,j+\frac{1}{2}}^{*,\pm} = \max\left(0, h_{\tau,j+\frac{1}{2}}^{n,\pm} + b_{\tau,j+\frac{1}{2}}^\pm - \max(b_{\tau,j+\frac{1}{2}}^+, b_{\tau,j+\frac{1}{2}}^-)\right), \tag{14}$$

which satisfies

$$h_{\tau,j+\frac{1}{2}}^{*,+} = h_{\tau,j+\frac{1}{2}}^{*,-}$$

at the steady state.

Now, let us discuss the well-balanced numerical fluxes. In the Lax–Friedrichs numerical flux $\widehat{F}_{j+1/2}$ defined in (9), the additional term $-\alpha(U_{\tau,j+\frac{1}{2}}^{n,+} - U_{\tau,j+\frac{1}{2}}^{n,-})$ contributes to the numerical viscosity, which is essential for this nonlinear conservation laws. However they may destroy the well-balanced property at the steady state. Therefore, we propose to modify this flux (9) as

$$\begin{aligned} &f\left(U_{\tau,j+\frac{1}{2}}^{n,-}, U_{\tau,j+\frac{1}{2}}^{n,+}; \sigma_{\tau,j+\frac{1}{2}}^-, \sigma_{\tau,j+\frac{1}{2}}^+\right) \\ &= \frac{1}{2}\left[\begin{pmatrix} \sigma^* h^{*,+} u^+ \\ \frac{(Q^+)^2}{H^+} + \frac{1}{2}g\sigma^+(h^+)^2 \end{pmatrix}_{\tau,j+\frac{1}{2}}^n \right. \\ &\quad + \begin{pmatrix} \sigma^* h^{*,-} u^- \\ \frac{(Q^-)^2}{H^-} + \frac{1}{2}g\sigma^-(h^-)^2 \end{pmatrix}_{\tau,j+\frac{1}{2}}^n \\ &\quad \left. -\alpha\left(\begin{pmatrix} \sigma^* h^{*,+} \\ Q^+ \end{pmatrix}_{\tau,j+\frac{1}{2}}^n - \begin{pmatrix} \sigma^* h^{*,-} \\ Q^- \end{pmatrix}_{\tau,j+\frac{1}{2}}^n\right)\right], \end{aligned} \tag{15}$$

where

$$\sigma_{\tau,j+\frac{1}{2}}^* = \min(\sigma_{\tau,j+\frac{1}{2}}^+, \sigma_{\tau,j+\frac{1}{2}}^-). \tag{16}$$

Here we modify the first component of the flux term from $Q_\tau^\pm$ to $\sigma_\tau^* h_\tau^{*,\pm} u_\tau^\pm$, for the purpose of positivity preserving to be explained in Section 3.

2.4. Source term approximation

Next, we present the high order well-balanced approximation to the source term integration. In Xing (2016), we designed high order well-balanced finite volume methods for the shallow water flows in channels, and the well-balanced approximation to the source term integration is obtained via an extrapolation technique. That approach can only provide even order approximation to the source term, and it is not easy to extend it to finite element methods. Here, a very different approach to approximate the source term is presented for our DG methods.

The source term of the momentum equation in (4) takes the form of

$$\int_{I_j} S^{(2)} v \mathrm{d}x = \frac{1}{2}g\int_{I_j}(h+b)^2\sigma_x v \mathrm{d}x - g\int_{I_j}(h+b)(\sigma b)_x v \mathrm{d}x + \frac{1}{2}g\int_{I_j}(\sigma b^2)_x v \mathrm{d}x, \tag{17}$$

where $S^{(2)}$ denote the second component of the source term. We can further decompose this integral as

$$\begin{aligned}\int_{I_j} S^{(2)} v\mathrm{d}x &= \frac{1}{2}g\int_{I_j}\left[(h+b)^2-\overline{(h+b)}_j^2\right]\sigma_x v\mathrm{d}x\\ &\quad -g\int_{I_j}\left[(h+b)-\overline{(h+b)}_j\right](\sigma b)_x v\mathrm{d}x\\ &\quad +\frac{1}{2}g\overline{(h+b)}_j^2\int_{I_j}\sigma_x v\mathrm{d}x - g\overline{(h+b)}_j\int_{I_j}(\sigma b)_x v\mathrm{d}x\\ &\quad +\frac{1}{2}g\int_{I_j}(\sigma b^2)_x v\mathrm{d}x.\\ &= \frac{1}{2}g\int_{I_j}\left[(h+b)^2-\overline{(h+b)}_j^2\right]\sigma_x v\mathrm{d}x\\ &\quad -g\int_{I_j}\left[(h+b)-\overline{(h+b)}_j\right](\sigma b)_x v\mathrm{d}x\\ &\quad +\frac{1}{2}g\overline{(h+b)}_j^2\left(\sigma v(x^-_{j+\frac{1}{2}})-\sigma v(x^+_{j-\frac{1}{2}})-\int_{I_j}\sigma v_x\mathrm{d}x\right)\\ &\quad -g\overline{(h+b)}_j\left(\sigma bv(x^-_{j+\frac{1}{2}})-\sigma bv(x^+_{j-\frac{1}{2}})-\int_{I_j}\sigma bv_x\mathrm{d}x\right)\\ &\quad +\frac{1}{2}g\left(\sigma b^2v(x^-_{j+\frac{1}{2}})-\sigma b^2v(x^+_{j-\frac{1}{2}})-\int_{I_j}\sigma b^2v_x\mathrm{d}x\right),\end{aligned} \tag{18}$$

by adding and subtracting the constant terms $\overline{(h+b)}_j^2$, $\overline{(h+b)}_j$ inside the integral, and applying integration by parts. Note that the constant term $\overline{(h+b)}_j$ can be replaced by any other term that can recover constant C at the still water steady state (2), for example $(h+b)(x_j)$.

Our numerical approximation to the source term (18) takes the following form

$$\begin{aligned}\int_{I_j} S^{(2)}_\tau v\mathrm{d}x &= \frac{1}{2}g\int_{I_j}\left[(h+b)^2_\tau-\overline{(h+b)}^2_{\tau,j}\right](\sigma_\tau)_x v\mathrm{d}x\\ &\quad -g\int_{I_j}\left[(h+b)_\tau-\overline{(h+b)}_{\tau,j}\right]((\sigma b)_\tau)_x v\mathrm{d}x\\ &\quad +\frac{1}{2}g\overline{(h+b)}^2_{\tau,j}\left(\{\sigma_\tau\}_{j+\frac{1}{2}}v^-_{j+\frac{1}{2}}-\{\sigma_\tau\}_{j-\frac{1}{2}}v^+_{j-\frac{1}{2}}-\int_{I_j}\sigma_\tau v_x\mathrm{d}x\right)\\ &\quad -g\overline{(h+b)}_{\tau,j}\left(\{(\sigma b)_\tau\}_{j+\frac{1}{2}}v^-_{j+\frac{1}{2}}-\{(\sigma b)_\tau\}_{j-\frac{1}{2}}v^+_{j-\frac{1}{2}}-\int_{I_j}(\sigma b)_\tau v_x\mathrm{d}x\right)\\ &\quad +\frac{1}{2}g\left(\left\{\frac{(\sigma b)^2_\tau}{\sigma_\tau}\right\}_{j+\frac{1}{2}}v^-_{j+\frac{1}{2}}-\left\{\frac{(\sigma b)^2_\tau}{\sigma_\tau}\right\}_{j-\frac{1}{2}}v^+_{j-\frac{1}{2}}-\int_{I_j}\frac{(\sigma b)^2_\tau}{\sigma_\tau}v_x\mathrm{d}x\right),\end{aligned} \tag{19}$$

where the terms σ, σb, σb^2, $h+b$, $\overline{(h+b)}_j$ are replaced by their numerical approximations σ_τ, $(\sigma b)_\tau$, $(\sigma b)^2_\tau/\sigma_\tau$, $(h+b)_\tau$, $\overline{(h+b)}_{\tau,j}$, respectively. Moreover, the boundary values of σ_τ, $(\sigma b)_\tau$, $(\sigma b)^2_\tau/\sigma_\tau$ are replaced by their averages at the cell interface, denoted by $\{\sigma_\tau\}$, $\{(\sigma b)_\tau\}$, $\left\{(\sigma b)^2_\tau/\sigma_\tau\right\}$, to be consistent with the numerical flux (15) at the steady state.

2.5. Slope limiter

For the system of hyperbolic conservation laws, when the solution contains discontinuities, DG methods are often coupled with a slope limiter procedure to compress the possible oscillation near the discontinuities. Many different choices of slope limiters are available in the literature, and we consider the classical total variation bounded (TVB) limiter (Shu, 1987) in this paper. The standard TVB limiter on the unknown U_τ involves two steps: the detection of the troubled-cell and the reconstruction of the polynomial solution in these troubled-cells.

The first step replies on the troubled-cell indicators which analyze the smoothness of the solution in the cell I_j based on the cell averages $\overline{U}_{\tau,j}$, $\overline{U}_{\tau,j\pm1}$ and cell boundary values $U^-_{\tau,j+1/2}$, $U^+_{\tau,j-1/2}$. Using these quantities, we can construct the forward and backward differences,

$$\begin{aligned}&\Delta_+\overline{U}_{\tau,j}=\overline{U}_{\tau,j+1}-\overline{U}_{\tau,j},\quad \Delta_-\overline{U}_{\tau,j}=\overline{U}_{\tau,j}-\overline{U}_{\tau,j-1},\\ &\widetilde{U}_{\tau,j}=U^-_{\tau,j+1/2}-\overline{U}_{\tau,j},\quad \overset{\approx}{U}_{\tau,j}=\overline{U}_{\tau,j}-U^+_{\tau,j-1/2}.\end{aligned} \tag{20}$$

The TVB limiter is applied to these differences to obtain

$$\begin{aligned}\widetilde{U}^{mod}_{\tau,j} &= m\left(\widetilde{U}_{\tau,j},\ \Delta_+\overline{U}_{\tau,j},\ \Delta_-\overline{U}_{\tau,j}\right),\\ \overset{\approx}{U}^{mod}_{\tau,j} &= m\left(\overset{\approx}{U}_{\tau,j},\ \Delta_+\overline{U}_{\tau,j},\ \Delta_-\overline{U}_{\tau,j}\right),\end{aligned}$$

where m is the minmod type TVB limiter:

$$m(b_1,b_2,\ldots,b_n) = \begin{cases} b_1, & \text{if } |b_1|\le M\Delta x^2,\\ \mathrm{sign}(b_1)\min\limits_{1\le i\le n}|b_i|, & \text{if } |b_1|>M\Delta x^2 \text{ and}\\ & \quad \mathrm{sign}(b_1)=\ldots=\mathrm{sign}(b_n),\\ 0, & \text{otherwise},\end{cases}$$

with M being the TVB parameter to be chosen adequately for each test and proportional to the second derivatives of the solution near smooth critical points. The cell interface values are then updated as

$$U^{-,mod}_{\tau,j+1/2}=\overline{U}_{\tau,j}+\widetilde{U}^{mod}_{\tau,j},\qquad U^{+,mod}_{\tau,j-1/2}=\overline{U}_{\tau,j}-\overset{\approx}{U}^{mod}_{\tau,j}, \tag{21}$$

and the cell I_j is marked as a troubled-cell if the update in (21) changes either of the two cell interface values, i.e., if $U^{-,mod}_{\tau,j+1/2}\neq U^-_{\tau,j+1/2}$ or $U^{+,mod}_{\tau,j-1/2}\neq U^+_{\tau,j-1/2}$.

If a cell is marked as a troubled-cell, the reconstruction step is to replace the polynomial in this cell by a limited linear or quadratic polynomial. For example, one can choose the limited function $U^{mod}_{\tau,j}$ as the unique quadratic polynomial satisfying (21) and also maintaining the original cell average $\overline{U}_{\tau,j}$.

For the system of conservation laws, we often apply the TVB limiter with local characteristic decomposition to achieve better numerical results, i.e., the variables are projected into the characteristic direction before evaluating the differences in (20). After we compute the updated cell interface values (21), we project them back to the physical spaces to detect the troubled-cells.

The standard limiter may conflict with the well-balanced property, and we propose a well-balanced limiter procedure following the idea presented in Xing et al. (2010) by modifying the troubled-cell detection step. In the proposed well-balanced slope limiter procedure, we will first check if the limiting is needed based on the cell averages $\overline{(h+b)}_{\tau,j}$, $\overline{(h+b)}_{\tau,j\pm1}$ and $(h+b)^-_{\tau,j+1/2}$, $(h+b)^+_{\tau,j-1/2}$. If the cell I_j is flagged as needing limiting, the actual TVB limiter is applied on U_τ as the above procedure. Note that $(h+b)_\tau$ becomes constant at the still water steady state (2), therefore, no limiter is applied when the steady state is reached, and the well-balanced property is maintained.

2.6. Summary of the well-balanced schemes

Our proposed well-balanced DG methods for the shallow water flows (1) in channels are given by (7), where the numerical fluxes are defined in (8) and (15), and the source term approximation is provided in (19). The method is completed by a temporal TVD Runge–Kutta discretization (10), with the well-balanced slope limiter procedure applied in each inner stage of the Runge–Kutta

methods. Collecting the results of the previous subsections, it is straightforward to prove the following result:

Proposition 1. *The DG methods for the shallow water flows in channels (1) as described above can maintain the well-balanced property for the steady state solutions (2).*

Proof. At the steady state (2), we have

$$(h+b)_\tau = C, \qquad Q_\tau = 0.$$

For the mass equation $H_t + Q_x = 0$, numerical approximation of the source term is 0, and the approximation of the flux term is $\widehat{F}^{(1)}_{j+\frac{1}{2}} v^-_{j+\frac{1}{2}} - \widehat{F}^{(1)}_{j-\frac{1}{2}} v^+_{j-\frac{1}{2}} - \int_{I_j} F^{(1)} v_x \mathrm{d}x$, where $F^{(1)} = Q_\tau$ stands for the flux term in the mass equation. Since $Q_\tau = 0$ at the steady state, the volume integral $\int_{I_j} F^{(1)} v_x \mathrm{d}x = 0$. Note that we have $h^{*,+}_{\tau,j+\frac{1}{2}} = h^{*,-}_{\tau,j+\frac{1}{2}}$ from (14), therefore the numerical flux $\widehat{F}^{(1)}$ as defined in (15) becomes zero too and there is no numerical dissipation.

Next, we prove the well-balanced property for the momentum equation which contains the source term. Denote the flux term in this equation by $F^{(2)}$. With the numerical flux given in (15), its numerical approximation on the left side of (7) takes the form of

$$\begin{aligned}&\widehat{F}^{(2)}_{j+\frac{1}{2}} v^-_{j+\frac{1}{2}} - \widehat{F}^{(2)}_{j-\frac{1}{2}} v^+_{j-\frac{1}{2}} - \int_{I_j} F^{(2)} v_x \mathrm{d}x \\ =&\frac{1}{2} g\{\sigma_\tau h_\tau^2\}_{j+\frac{1}{2}} v(x^-_{j+\frac{1}{2}}) - \frac{1}{2} g\{\sigma_\tau h_\tau^2\}_{j-\frac{1}{2}} v(x^+_{j-\frac{1}{2}}) - \int_{I_j} \frac{1}{2} g\sigma_\tau h_\tau^2 v_x \mathrm{d}x.\end{aligned} \tag{22}$$

Since $(h+b)_\tau = \overline{(h+b)}_{\tau,j} \equiv C$, the source term approximation (19) becomes

$$\begin{aligned}\int_{I_j} S^{(2)}_\tau v \mathrm{d}x = &\frac{1}{2} gC^2 \left(\{\sigma_\tau\}_{j+\frac{1}{2}} v^-_{j+\frac{1}{2}} - \{\sigma_\tau\}_{j-\frac{1}{2}} v^+_{j-\frac{1}{2}} - \int_{I_j} \sigma_\tau v_x \mathrm{d}x \right) \\ &- gC \left(\{(\sigma b)_\tau\}_{j+\frac{1}{2}} v^-_{j+\frac{1}{2}} - \{(\sigma b)_\tau\}_{j-\frac{1}{2}} v^+_{j-\frac{1}{2}} - \int_{I_j} (\sigma b)_\tau v_x \mathrm{d}x \right) \\ &+ \frac{1}{2} g \left(\{\sigma_\tau b_\tau^2\}_{j+\frac{1}{2}} v^-_{j+\frac{1}{2}} - \{\sigma_\tau b_\tau^2\}_{j-\frac{1}{2}} v^+_{j-\frac{1}{2}} - \int_{I_j} \sigma_\tau b_\tau^2 v_x \mathrm{d}x \right).\end{aligned}$$

Notice the equality that

$$\begin{aligned}\frac{1}{2} g\sigma_\tau h_\tau^2 &= \frac{1}{2} g\sigma_\tau (h+b)_\tau^2 - g\sigma_\tau (h+b)_\tau b_\tau + \frac{1}{2} g\sigma_\tau b_\tau^2 \\ &= \frac{1}{2} gC^2 \sigma_\tau - gC\sigma_\tau b_\tau + \frac{1}{2} g\sigma_\tau b_\tau^2,\end{aligned} \tag{23}$$

therefore, we can conclude that the flux and source term approximations balance each other at the still water steady state, which leads to the desired well-balanced property. □

3. Positivity-preserving methods

Zhang and Shu (2010) proposed a framework to design high order maximum-principle-preserving methods for hyperbolic conservation laws. Since then, the method has gained many attentions, and has been applied to various applications, including the shallow water equations in Xing (2016), Xing and Zhang (2013) and Xing et al. (2010). It was shown to be able to maintain the non-negativity of water height under suitable CFL condition without affecting the mass conservation, and keep the high order accuracy for the general solutions. Here, we will explore the application of this approach to the well-balanced DG methods presented in Section 2 for the shallow water flows in open channels.

As explained in Zhang and Shu (2010), the key components to achieve this goal are the following two items: the positivity of the first order version of this method, and a simple positivity-preserving limiter to be coupled with the high order method. Following the setup, we only consider the simple Euler time discretization, and the same results can be generalized to multi-step and TVD high order Runge–Kutta methods. Without loss of generality, we ignore the subscript τ in this section. Consider the well-balanced DG methods (7) with the numerical fluxes defined in (15), take the test function $v = 1$ leads to the following update of the cell averages of the wet cross section

$$\overline{H}^{n+1}_j = \overline{H}^n_j - \lambda \left[\widehat{F}^{(1)}_{j+\frac{1}{2}} - \widehat{F}^{(1)}_{j-\frac{1}{2}} \right], \tag{24}$$

where

$$\begin{aligned}\widehat{F}^{(1)}_{j+\frac{1}{2}} = &\frac{1}{2} \Big[\sigma^*_{j+\frac{1}{2}} h^{*,-}_{j+\frac{1}{2}} u^{n,-}_{j+\frac{1}{2}} + \sigma^*_{j+\frac{1}{2}} h^{*,+}_{j+\frac{1}{2}} u^{n,+}_{j+\frac{1}{2}} \\ &- \alpha \left(\sigma^*_{j+\frac{1}{2}} h^{*,+}_{j+\frac{1}{2}} - \sigma^*_{j+\frac{1}{2}} h^{*,-}_{j+\frac{1}{2}} \right) \Big],\end{aligned} \tag{25}$$

and $\lambda = \Delta t/\Delta x$. The first order version of this method takes the form of

$$H^{n+1}_j = H^n_j - \lambda \left[\widehat{F}^{(1)}_{j+\frac{1}{2}} - \widehat{F}^{(1)}_{j-\frac{1}{2}} \right], \tag{26}$$

with the numerical flux defined as

$$\begin{aligned}\widehat{F}^{(1)}_{j+\frac{1}{2}} = &\frac{1}{2} \Big[\sigma^*_{j+\frac{1}{2}} h^{*,-}_{j+\frac{1}{2}} u^n_j + \sigma^*_{j+\frac{1}{2}} h^{*,+}_{j+\frac{1}{2}} u^n_{j+1} \\ &- \alpha \left(\sigma^*_{j+\frac{1}{2}} h^{*,+}_{j+\frac{1}{2}} - \sigma^*_{j+\frac{1}{2}} h^{*,-}_{j+\frac{1}{2}} \right) \Big],\end{aligned} \tag{27}$$

and the first order version of the starred terms $h^{*,\pm}_{j+\frac{1}{2}}$, $\sigma^*_{j+\frac{1}{2}}$ given by

$$\begin{aligned}h^{*,-}_{j+\frac{1}{2}} &= \max\left(0, h^n_j + b_j - \max(b_j, b_{j+1})\right), \\ h^{*,+}_{j+\frac{1}{2}} &= \max\left(0, h^n_{j+1} + b_{j+1} - \max(b_j, b_{j+1})\right), \\ \sigma^*_{j+\frac{1}{2}} &= \min(\sigma_j, \sigma_{j+1}).\end{aligned} \tag{28}$$

We have the following lemma about the positivity-preserving property of this first order method.

Lemma 2. *Under the CFL condition $\lambda\alpha \le 1$ with $\alpha = \max(|u| + \sqrt{gh})$, consider the first order scheme (26) with the numerical flux (27) and (28). If $H^n_j, H^n_{j\pm1}$ are non-negative, then H^{n+1}_j is also non-negative.*

Proof. The scheme (26) can be written as

$$\begin{aligned}H^{n+1}_j = &\left[1 - \frac{1}{2}\lambda\left(\alpha + u^n_j\right) \frac{\sigma^*_{j+\frac{1}{2}}}{\sigma_j} \frac{h^{*,-}_{j+\frac{1}{2}}}{h^n_j} \right. \\ &\left. - \frac{1}{2}\lambda\left(\alpha - u^n_j\right) \frac{\sigma^*_{j-\frac{1}{2}}}{\sigma_j} \frac{h^{*,+}_{j-\frac{1}{2}}}{h^n_j} \right] \sigma_j h^n_j \\ &+ \frac{1}{2}\lambda\left(\alpha + u^n_{j-1}\right) \sigma^*_{j-\frac{1}{2}} h^{*,-}_{j-\frac{1}{2}} + \frac{1}{2}\lambda\left(\alpha - u^n_{j+1}\right) \sigma^*_{j+\frac{1}{2}} h^{*,+}_{j+\frac{1}{2}} \\ \ge &\left[1 - \frac{1}{2}\lambda(\alpha + u^n_j) - \frac{1}{2}\lambda(\alpha - u^n_j) \right] \sigma_j h^n_j \\ &+ \frac{1}{2}\lambda\left(\alpha + u^n_{j-1}\right) \sigma^*_{j-\frac{1}{2}} h^{*,-}_{j-\frac{1}{2}} + \frac{1}{2}\lambda\left(\alpha - u^n_{j+1}\right) \sigma^*_{j+\frac{1}{2}} h^{*,+}_{j+\frac{1}{2}} \\ = &(1 - \lambda\alpha)\sigma_j h^n_j + \frac{1}{2}\lambda\left(\alpha + u^n_{j-1}\right) \sigma^*_{j-\frac{1}{2}} h^{*,-}_{j-\frac{1}{2}} \\ &+ \frac{1}{2}\lambda\left(\alpha - u^n_{j+1}\right) \sigma^*_{j+\frac{1}{2}} h^{*,+}_{j+\frac{1}{2}},\end{aligned}$$

since $0 \le h^{*,-}_{j+\frac{1}{2}}, h^{*,+}_{j-\frac{1}{2}} \le h^n_j$ and $\sigma^*_{j\pm\frac{1}{2}} \le \sigma_j$ (this also justifies the reason that we pick the minimum value in the definition of σ^* in (16)). Therefore, H^{n+1}_j is a linear combination of h^n_{j-1}, $h^{*,-}_{j-\frac{1}{2}}$ and $h^{*,+}_{j+\frac{1}{2}}$ and all the coefficients are non-negative, which leads to $H^{n+1}_j \ge 0$. □

Next, we move to discuss high order schemes. We refer to Zhang and Shu (2010) and Xing et al. (2010) for the details and only present the main idea here. We introduce the N-point (with $2N-3 \geq k$) Legendre Gauss-Lobatto quadrature rule on the interval I_j, and denote these quadrature points by $\mathcal{S}_j = \left\{x_{j-\frac{1}{2}} = \hat{x}_j^1, \hat{x}_j^2, \cdots, \hat{x}_j^{N-1}, \hat{x}_j^N = x_{j+\frac{1}{2}}\right\}$, with the corresponding quadrature weights $\widehat{w}_r$ for the interval $[-1/2, 1/2]$ satisfying $\sum_{r=1}^{N} \widehat{w}_r = 1$. We employ the following positivity-preserving limiter (Xing et al., 2010; Zhang and Shu, 2010) on the DG polynomial $U_j^n(x) = (H_j^n(x), Q_j^n(x))^T$,

$$\widetilde{U}_j^n(x) = \theta\left(U_j^n(x) - \overline{U}_j^n\right) + \overline{U}_j^n, \qquad \theta = \min\left\{1, \frac{\overline{H}_j^n}{\overline{H}_j^n - m_j}\right\}, \tag{29}$$

with

$$m_j = \min_{x \in S_j} H_j^n(x) = \min_{r=1,\cdots,N} H_j^n(\hat{x}_j^r). \tag{30}$$

With this choice of m_j, we can show that $\widetilde{H}_j^n(\hat{x}_j^r) \geq 0\ (r = 1, \cdots, N)$, and this limiter maintains the local conservation of the variable $U_j^n(x)$.

We compute the modified polynomial $\widetilde{U}_j^n(x)$ and use $\widetilde{U}_j^n(x)$ instead of $U_j^n(x)$ in the well-balanced methods (7). Following the proofs in Xing et al. (2010) and Zhang and Shu (2010), we can verify that the well-balanced methods coupled with this positivity-preserving limiter are high order accurate, positivity-preserving and mass conservation, under the CFL condition

$$\lambda\alpha \leq \widehat{w}_1. \tag{31}$$

To be efficient, we could implement the time step restriction (31) only when a preliminary calculation to the next time step produces negative wet cross section.

4. Numerical examples

In this section, we carry out extensive numerical experiments to demonstrate the performance of the proposed positivity-preserving well-balanced DG methods for the shallow water flows in open channels. The third order finite element DG methods (i.e., $k = 2$), coupled with third order TVD Runge–Kutta methods (10), are implemented in these examples. The CFL number is taken as 0.16 which satisfies the requirement (31) to achieve positivity-preserving property. The gravitation constant g is fixed as $9.812\,\mathrm{m/s^2}$. Channels with both continuous and discontinuous width functions have been tested.

4.1. Accuracy test

We first test the third order accuracy of the resulting method on an example with smooth solutions. The following periodic bottom topography and channel width function

$$b(x) = \sin^2(\pi x), \quad \sigma(x) = e^{\sin(2\pi x)},$$

are considered in this example. The initial conditions are given by

$$h(x,0) = 3 + e^{\cos(2\pi x)}, \quad Q(x,0) = \sin(\cos(2\pi x)), \quad x \in [0,1],$$

with periodic boundary conditions. We run the test up to the stopping time $t = 0.1$ when the solutions are still smooth.

As the exact solutions are not available for this nonlinear system, we apply the same method with a much refined $N = 25{,}600$ cells to obtain a reference solution, and then treat it as the exact solution when computing the errors and convergence rates, which are shown in Table 1. We can clearly observe that the expected third order accuracy is achieved.

Table 1
L^1 errors and orders for the test case in Section 4.1.

Cells	H		Q	
	L^1 error	Order	L^1 error	Order
25	1.19E−04		9.53E−05	
50	1.47E−05	3.02	1.16E−05	3.03
100	1.85E−06	2.99	1.46E−06	2.99
200	2.33E−07	2.99	1.84E−07	2.99
400	2.93E−08	2.99	2.31E−08	2.99
800	3.64E−09	3.01	2.87E−09	3.01
1600	4.58E−10	2.99	3.62E−10	2.99

4.2. Well-balanced test

The purpose of the second test problem (Balbas and Karni, 2009; Xing, 2016) is to verify the well-balanced property of our proposed DG methods. We consider the bottom topography given by

$$b(x) = \begin{cases} 0.25(1 + \cos(10\pi(x - 0.5))), & \text{if } 0.4 \leq x \leq 0.6, \\ 0, & \text{otherwise}, \end{cases} \tag{32}$$

in the domain [0, 1]. The channel with varying width $\sigma(x)$ takes the form of

$$\sigma(x) = \begin{cases} 1 - \sigma_0\left(1 + \cos\left(2\pi\dfrac{x - (x_l + x_r)/2}{x_r - x_l}\right)\right), & \text{if } x \in [x_l, x_r], \\ 1, & \text{otherwise}, \end{cases} \tag{33}$$

where x_l and x_r are the left and right boundary of the contraction, and $1 - 2\sigma_0$ represents the minimum width of the channel at the point $(x_l + x_r)/2$. In this example, we choose $x_l = 0.25, x_r = 0.75$, and $\sigma_0 = 0.2$. The initial condition is provided as the steady state solution

$$h + b = 1, \quad Q = \sigma hu = 0,$$

and the periodic boundary condition is considered.

We solve the problem with 200 uniform cells until the final time $T = 1$. The numerical surface level $h + b$ and the bottom b are plotted in Fig. 1. The 3D plot of the bottom topography b and the channel shape σ is provided in Fig. 2. In order to demonstrate that the steady state solution is maintained up to round-off error, the L^1, L^2 and L^∞ errors of the wet cross section H and the mass flow rate Q with single precision and double-precision are shown in Table 2. We can clearly see that the L^1, L^2 and L^∞ errors are all at the level of round-off errors for these precisions, which verify the expected well-balanced property.

4.3. Small perturbation test

In this subsection, we simulate the propagation of small perturbations to a steady state solution, to demonstrate the capability of the proposed DG methods for such challenging case. This test was first proposed by Balbas and Karni (2009). We set the bottom topography as (32), and the initial condition as

$$h + b = \begin{cases} 1 + 0.01, & \text{if } 0.1 \leq x \leq 0.2, \\ 1, & \text{otherwise}, \end{cases} \quad Q = \sigma hu = 0,$$

in a computational domain [0, 1] with simple transmissive boundary conditions. Two different sets of channel $\sigma(x)$ defined in (33) are tested, one with a left shifted contraction $x_l = 0.15, x_r = 0.65, \sigma_0 = 0.2$, and the other with a right shifted contraction $x_l = 0.35, x_r = 0.85, \sigma_0 = 0.2$.

For these tests involving such small perturbation of steady state solutions, non-well-balanced numerical methods usually have

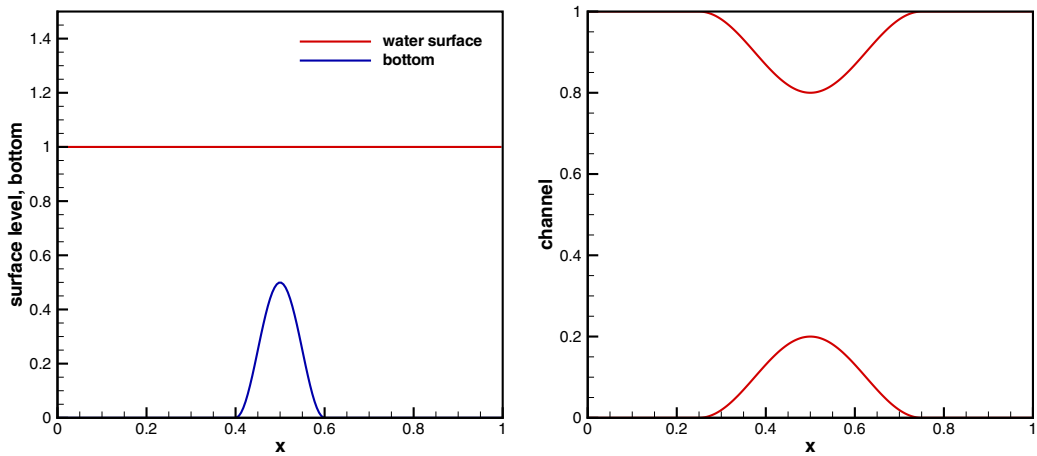

Fig. 1. The still water steady state solution in Section 4.2. Left: the surface level $h + b$ and the bottom topography b; Right: the shape σ of the channel.

Table 2
L^1, L^2 and L^∞ errors of the still water steady state solutions in Section 4.2.

Precision	L^1 error		L^2 error		L^∞ error	
	H	Q	H	Q	H	Q
Single	4.50E−08	1.54E−06	3.73E−09	1.35E−07	1.19E−07	5.36E−06
Double	2.66E−17	2.85E−15	4.08E−18	2.50E−16	2.22E−16	9.68E−15

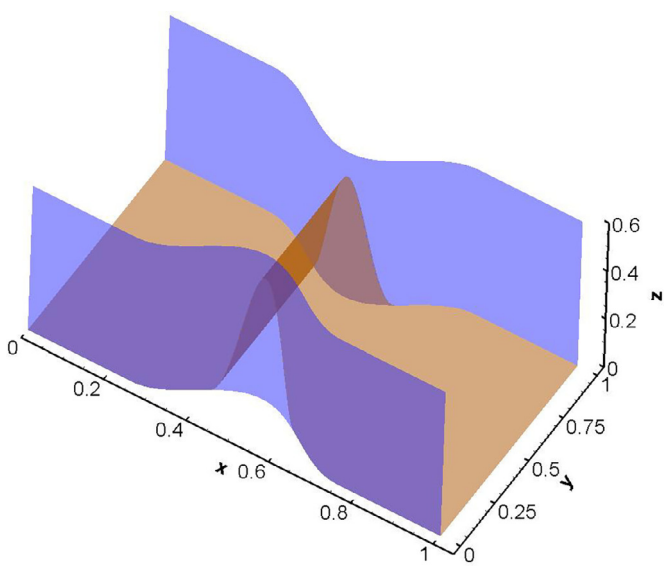

Fig. 2. The 3D plot of the bottom topography b and the channel shape σ in Section 4.2.

difficulty with the calculations and produce oscillatory results (Kurganov and Levy, 2002). The numerical results of the proposed well-balanced DG methods at different times on 200 uniform computational cells, compared with refined 2000 cells "reference" solutions, are shown in Fig. 3. For the sake of comparison, we also present the numerical results by the non-well-balanced DG methods with 200 cells. We can clearly observe that the well-balanced results are free of spurious numerical oscillations, and our methods can numerically capture such small perturbation well on relatively coarse meshes.

4.4. A converging-diverging channel

Here we consider the classic transcritical steady flow in a converging-diverging channel, originally proposed by García-Navarro et al. (1992). This test is related to many practical problems such as the flow between bridge piers. The bottom is set as flat (i.e., $b = 0$), and the converging-diverging channel is given by

$$\sigma(x) = \begin{cases} 5 - 0.7065\left(1 + \cos\left(2\pi \dfrac{x - 250}{300}\right)\right), & \text{if } x \in [150, 450], \\ 5, & \text{otherwise}, \end{cases}$$

in the computational domain $[0, 500]$. The initial conditions are set as

$$h = 2, \;\; Q = \sigma h u = 20,$$

and the boundary conditions are given by $Q = 20$ at the upstream, and $h = 1.85$ at the downstream. We compute this test up to a long time $T = 5000$ (until it reaches a steady state) using 200 uniform cells, and present the numerical result of the water height h in Fig. 4, which agrees well with those in the literature (García-Navarro et al., 1992; Vázquez-Céndon, 1999). The flow changes from subcritical flow to supercritical flow at the critical point ($x = 250$), and later becomes subcritical flow via a stationary hydraulic jump to connect to the subcritical downstream boundary condition.

4.5. Drain on a non-flat bottom

In this section, we consider a drainage test, first proposed by Gallouët et al. (2003) and later appeared in Xing and Shu (2011) for the shallow water equations. The goal is to test both well-balanced property and positivity-preserving feature of our methods.

The bottom topography is given by

$$b(x) = \begin{cases} 0.2 - 0.05(x - 10)^2, & \text{if } 8 \le x \le 12, \\ 0, & \text{otherwise}, \end{cases}$$

on the computational domain [0, 25], and the channel width is set as

$$\sigma(x) = \begin{cases} 1 - 0.2\left(1 + \cos\dfrac{2\pi(x - 10)}{12.5}\right), & \text{if } 3.75 \le x \le 10, \\ 1, & \text{otherwise}, \end{cases}$$

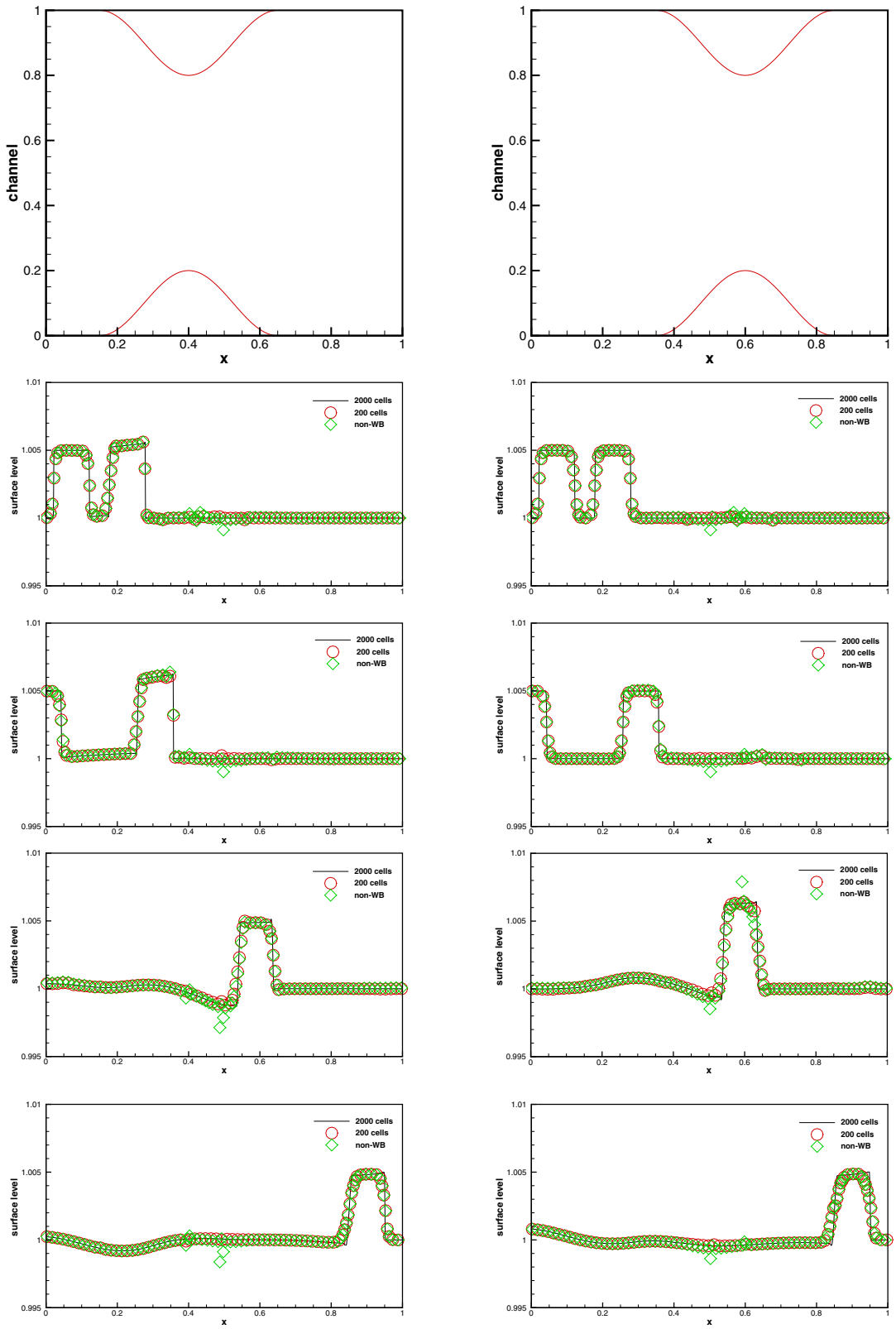

Fig. 3. The contracting channel $\sigma(x)$ (the top row) and numerical results by well-balanced DG methods with 200 and 2000 cells as well as those by non-well-balanced (denoted by "non-WB") DG methods with 200 cells at $T = 0.025, 0.05, 0.15$ and 0.25 (from top to bottom) in Section 4.3. Left: the channel with a left shifted contraction; Right: the channel with a right shifted contraction.

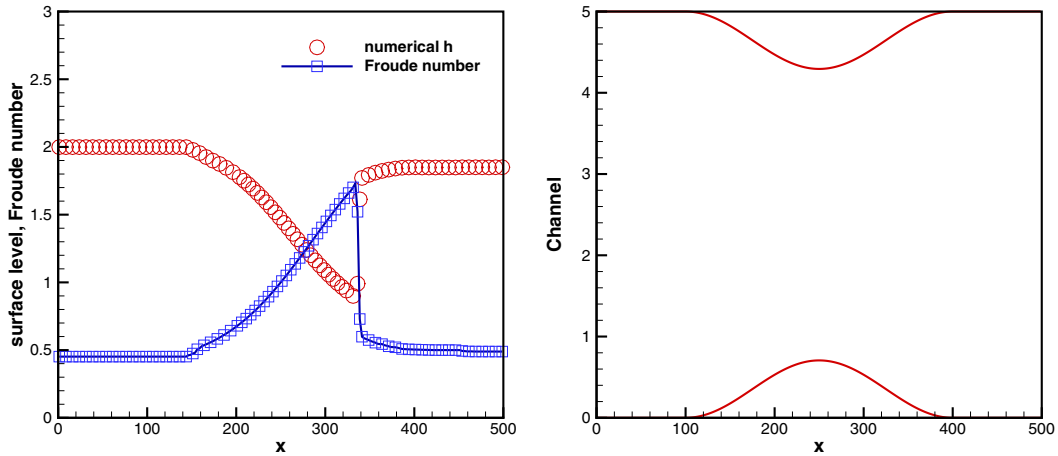

Fig. 4. Steady transcritical flow in a converging-diverging channel (left) and the channel shape $\sigma(x)$ (right) in Section 4.4.

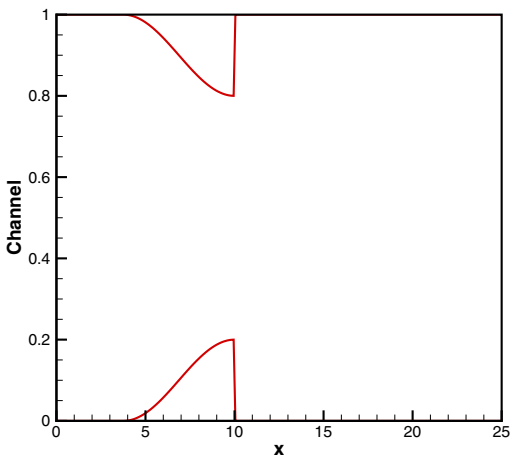

Fig. 5. The discontinuous channel $\sigma(x)$ in Section 4.5.

which is discontinuous at the point $x = 10$, and is shown in Fig. 5.

We consider the initial conditions as follows:

$$h(x,0) = 0.5 - b(x), \quad H(x,0) = \sigma(x)h(x,0), \quad Q(x,0) = 0.$$

A free boundary condition on H and zero on Q is imposed on the left boundary, and an outlet condition on a dry bed (refer to Gallouët et al., 2003 for the details) is used on the right boundary. A uniform mesh with 250 cells is taken. We present the water surface level $h + b$ and the discharge Q at $T = 10, 20, 100$ and 500 in Fig. 6, respectively. We can observe that the numerical solution reaches the steady state after a long time. The converged steady state is a still water (requiring well-balanced feature of the numerical methods) on the left of the bump, and a dry state (requiring positivity-preserving feature of the numerical methods) on the right of the bump. The numerical results show that our proposed DG methods work well for this challenging test even with a discontinuous channel.

4.6. Moving water steady states over a hump

In this last numerical example (Xing, 2016), we consider the convergence of our methods towards steady transcritical and subcritical flows with different channel configurations. In Xing and Shu (2006), the same tests are used to check the performance of well-balanced DG methods for the shallow water equations (i.e., constant channel width). The computational domain is set as [0, 25] and the bottom topography is defined by

$$b(x) = \begin{cases} 0.2 - 0.05(x-10)^2, & \text{if } 8 \le x \le 12, \\ 0, & \text{otherwise}, \end{cases}$$

We choose different sets of variable channel width, to be defined in each case, to demonstrate the effect of channel on the final so-

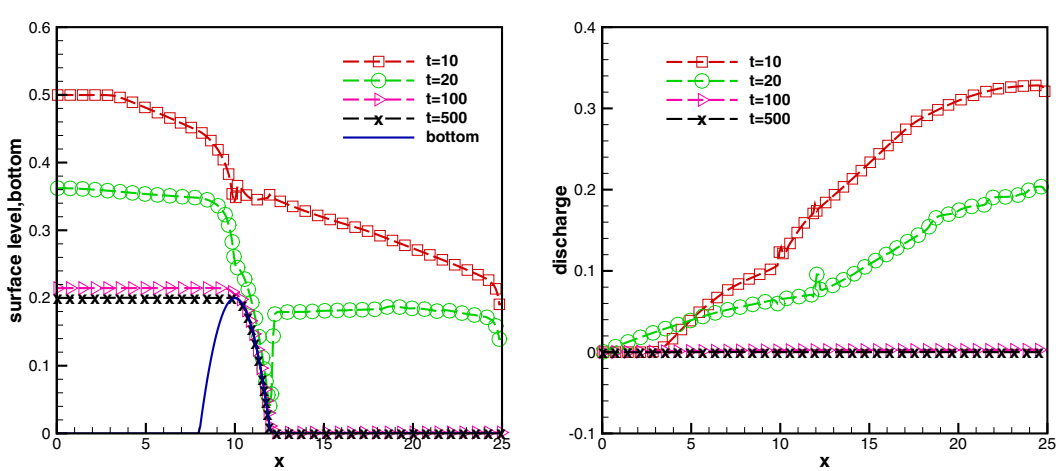

Fig. 6. Drain on a non-flat bottom with a discontinuous channel in Section 4.5. Left: the surface level $h + b$ at different times and bottom; Right: The discharge Q at different times.

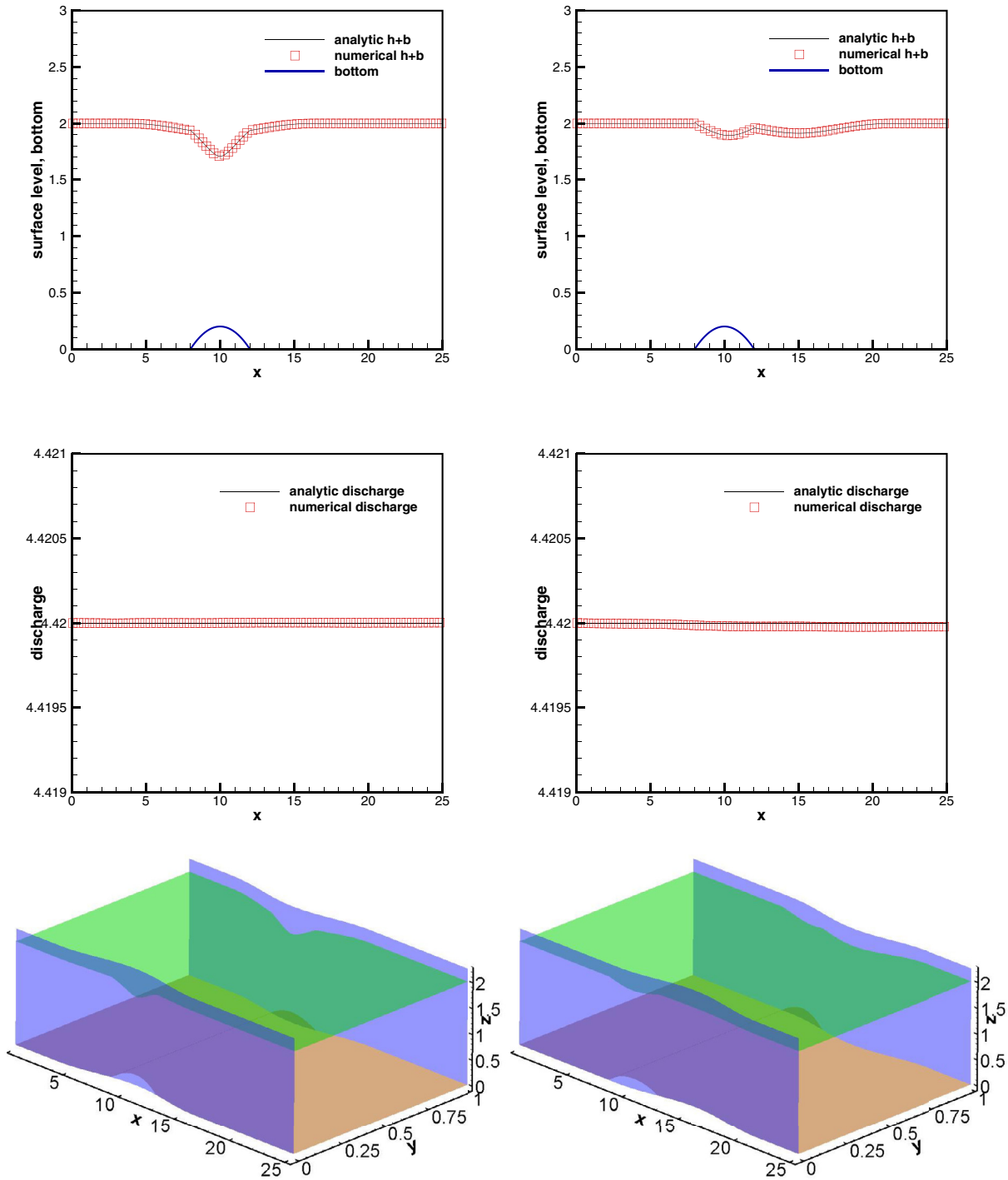

Fig. 7. Steady subcritical flow over a bump in Section 4.6. Top: the surface level $h+b$; Middle: the discharge Q as the numerical flux for the water height H; Bottom: the 3D plot of the bottom b, water surface $h+b$ and channel shape σ; Left: the channel with a left shifted contraction; Right: the channel with a right shifted contraction.

lutions. The initial conditions are given by

$$h(x,0) = 0.5 - b(x), \quad Q(x,0) = 0.$$

We take 200 uniform computational cells and set the final time as $T = 200$ when the flow reaches moving water steady states. Depending on different boundary conditions, the flow can be subcritical or transcritical with or without a steady shock. Analytical solutions for these moving water steady states can be computed, and will be provided for comparison.

4.6.1. Subcritical flow

The boundary condition is set as $hu = 4.42$ at the upstream, and $h = 2$ at the downstream. Two different sets of channel width $\sigma(x)$, defined in (33), are considered in this case, one with a left shifted contraction $x_l = 3.75, x_r = 16.25, \sigma_0 = 0.05$, and the other with a right shifted contraction $x_l = 8.75, x_r = 21.25, \sigma_0 = 0.05$. The flow will evolve to a moving water steady state at time $T = 200$. The converged state is a subcritical flow. We show the surface level $h+b$ and the mass flow rate Q at the final time in Fig. 7, and also include the analytical solutions in them for comparison. It is clear

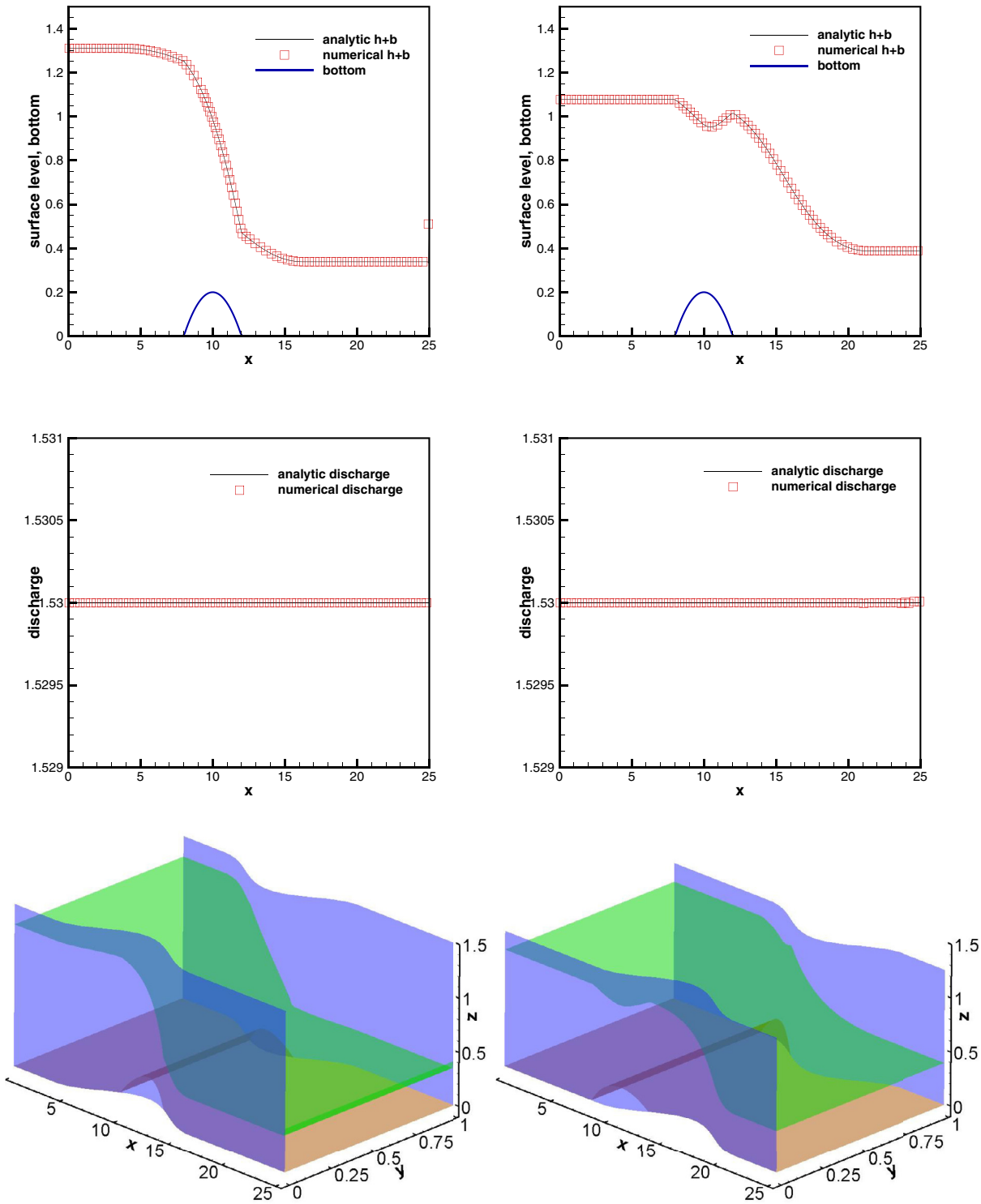

Fig. 8. Steady subcritical flow over a bump without a shock in Section 4.6. Top: the surface level $h+b$; Middle: the discharge Q as the numerical flux for the water height H; Bottom: the 3D plot of the bottom b, water surface $h+b$ and channel shape σ; Left: the channel with a left shifted contraction; Right: the channel with a right shifted contraction.

that the numerical solutions are in good agreement with the analytic ones. We can also observe the effect of different $\sigma(x)$ on the converged steady state solutions.

4.6.2. Transcritical flow without a shock

The boundary condition is set as $hu = 1.53$ at the upstream, and $h = 0.66$ at the downstream. Two different sets of channel $\sigma(x)$, defined in (33), are considered, one with a left shifted contraction $x_l = 3.75, x_r = 16.25, \sigma_0 = 0.15$, and the other with a right shifted contraction $x_l = 8.75, x_r = 21.25, \sigma_0 = 0.15$. The converged steady state solution is a transcritical flow without a shock. The surface level $h+b$ and the mass flow rate Q are plotted in Fig. 8, which show very good agreement with the analytical solutions.

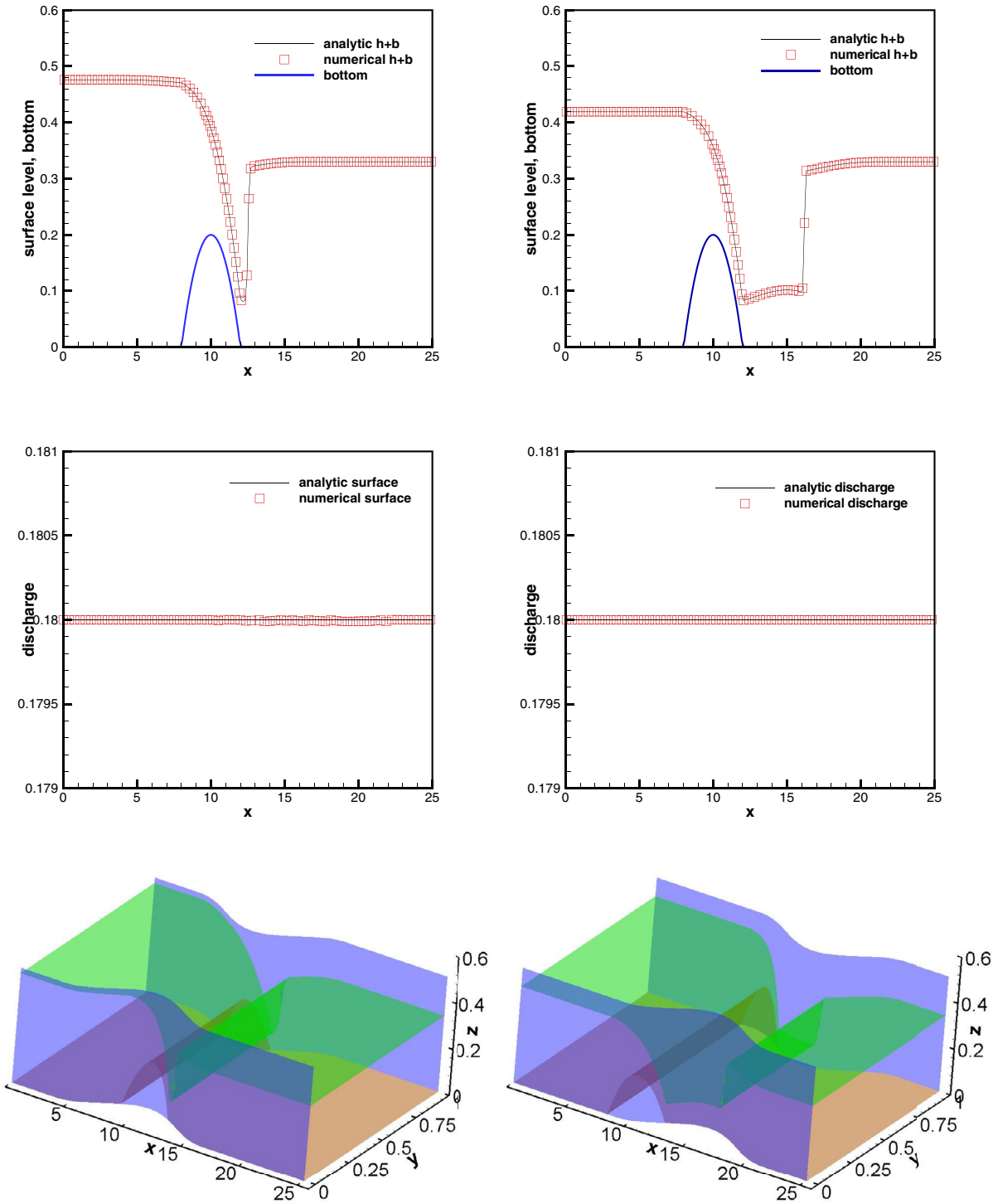

Fig. 9. Steady subcritical flow over a bump with a shock in Section 4.6. Top: the surface level $h+b$; Middle: the discharge Q as the numerical flux for the water height H; Bottom: the 3D plot of the bottom b, water surface $h+b$ and channel shape σ; Left: the channel with a left shifted contraction; Right: the channel with a right shifted contraction.

4.6.3. Transcritical flow with a shock

The boundary condition is set as $hu = 0.18$ at the upstream, and $h = 0.33$ at the downstream. Two different sets of channel $\sigma(x)$, defined in (33), are considered, one with a left shifted contraction $x_l = 3.75, x_r = 16.25, \sigma_0 = 0.15$, and the other with a right shifted contraction $x_l = 8.75, x_r = 21.25, \sigma_0 = 0.15$. The converged steady state solution is a transcritical flow with a shock appearing in the middle of the domain. We present the surface level $h+b$ and the mass flow rate Q in Fig. 9, which agree well with the analytical solutions.

5. Conclusions

Efficient DG methods have been designed in this paper for the shallow water flows in open channels with a non-flat bottom topography. The proposed methods have two nice features: well-balanced for the still water steady state solutions and positivity-preserving near the wetting and drying front. The well-balanced property is achieved via a novel source term splitting and appropriate well-balanced approximation of each split source term. A simple positivity-preserving limiter, adopted from Zhang and Shu (2010), was used to ensure the resulting methods maintain the non-negativity of the cross sectional wet area. We have carried out extensive numerical simulations, which demonstrate that the proposed methods are well-balanced, efficient for the small perturbation test near the steady state solutions, positivity-preserving near the wetting and drying front, high order accurate, and also perform well for both continuous and discontinuous solutions. Future work include the extension to the generalized model with the channel width σ depending on both x and z.

Acknowledgments

The second author (G. Li) acknowledges the support of the National Natural Science Foundation of China through Grants 11771228. The third author (F. Shao) was supported by the National Natural Science Foundation of China through Grants 41476101. The work of the last author (Y. Xing) was partially supported by the NSF grant DMS-1753581 and ONR grant N00014-16-1-2714.

References

Audusse, E., Bouchut, F., Bristeau, M.O., Klein, R., Perthame, B., 2004. A fast and stable well-balanced scheme with hydrostatic reconstruction for shallow water flows. SIAM J. Sci. Comput. 25, 2050–2065.
Balbás, J., Hernández-Duenas, G., 2014. A positivity preserving central scheme for shallow water flows in channels with wet-dry states. ESAIM Math. Modell. Numer. Anal. 48, 665–696.
Balbas, J., Karni, S., 2009. A central scheme for shallow water flows along channels with irregular geometry. ESAIM Math. Modell. Numer. Anal. 43, 333–351.
Bermudez, A., Vazquez, M.E., 1994. Upwind methods for hyperbolic conservation laws with source terms. Comput. Fluids 23, 1049–1071.
Bokhove, O., 2005. Flooding and drying in discontinuous galerkin finite-element discretizations of shallow-water equations. part 1: one dimension. J. Sci. Comput. 22, 47–82.
Bunya, S., Kubatko, E.J., Westerink, J.J., Dawson, C., 2009. A wetting and drying treatment for the Runge-Kutta discontinuous Galerkin solution to the shallow water equations. Comput. Methods Appl. Mech. Eng. 198, 1548–1562.
Cockburn, B., Karniadakis, G., Shu, C.W., 2000. The development of discontinuous Galerkin methods. In: Cockburn, B., Karniadakis, G., Shu, C.W. (Eds.), Discon-tinuous Galerkin Methods: Theory, Computation and Applications. In: Lecture Notes in Computational Science and Engineering, Part I: Overview, vol. 11. Springer, pp. 3–50.
Ern, A., Piperno, S., Djadel, K., 2008. A well-balanced Runge-Kutta discontinuous Galerkin method for the shallow-water equations with flooding and drying. Int. J. Numer. Methods Fluids 58, 1–25.
Gallouët, T., Hérard, J.M., Seguin, N., 2003. Some approximate Godunov schemes to compute shallow-water equations with topography. Comput. Fluids 32, 479–513.
García-Navarro, P., Alcrudo, F., Savirón, J., 1992. 1D open channel flow simulation using TVD-mccormack scheme. J. Hydraul. Eng. 118, 1359–1372.
García-Navarro, P., Vázquez-Céndon, M.E., 2000. On numerical treatment of the source terms in the shallow water equations. Comput. Fluids 29, 951–979.
Greenberg, J.M., LeRoux, A.Y., 1996. A well-balanced scheme for the numerical processing of source terms in hyperbolic equations. SIAM J. Numer. Anal. 33, 1–16.
Hernández-Duenas, G., Beljadid, A., 2016. A central-upwind scheme with artificial viscosity for shallow-water flows in channels. Adv. Water Resour. 96, 323–338.
Hernández-Duenas, G., Karni, S., 2011. Shallow water flows in channels. J. Sci. Comput. 48, 190–208.
Kurganov, A., Levy, D., 2002. Central-upwind schemes for the saint-venant system. ESAIM Math. Modell. Numer. Anal. 36, 397–425.
LeVeque, R.J., 1998. Balancing source terms and flux gradients on high-resolution Godunov methods: the quasi-steady wave-propagation algorithm. J. Comput. Phys. 146, 346–365.
Murillo, J., García-Navarro, P., 2014. Accurate numerical modeling of 1d flow in channels with arbitrary shape. Application of the energy balanced property. J. Comput. Phys. 260, 222–248.
Perthame, B., Simeoni, C., 2001. A kinetic scheme for the Saint-Venant system with a source term. Calcolo 38, 201–231.
Shu, C.W., 1987. TVB uniformly high-order schemes for conservation laws. Math. Comput. 49, 105–121.
Shu, C.W., 1988. Total-variation-diminishing time discretizations. SIAM J. Sci. Stat. Comput. 9, 1073–1084.
Vázquez-Céndon, M.E., 1999. Improved treatment of source terms in upwind schemes for the shallow water equations in channels with irregular geometry. J. Comput. Phys. 148, 497–526.
Xing, Y., 2014. Exactly well-balanced discontinuous Galerkin methods for the shallow water equations with moving water equilibrium. J. Comput. Phys. 257, 536–553.
Xing, Y., 2016. High order finite volume WENO schemes for the shallow water flows through channels with irregular geometry. J. Comput. Appl. Math. 299, 229–244.
Xing, Y., Shu, C.W., 2005. High order finite difference WENO schemes with the exact conservation property for the shallow water equations. J. Comput. Phys. 208, 206–227.
Xing, Y., Shu, C.W., 2006. High order well-balanced finite volume WENO schemes and discontinuous Galerkin methods for a class of hyperbolic systems with source terms. J. Comput. Phys. 214, 567–598.
Xing, Y., Shu, C.W., 2011. High-order finite volume WENO schemes for the shallow water equations with dry states. Adv Water Resour 34, 1026–1038.
Xing, Y., Shu, C.W., 2013. High order well-balanced WENO scheme for the gas dynamics equations under gravitational fields. J. Sci. Comput. 54, 645–662.
Xing, Y., Zhang, X., 2013. Positivity-preserving well-balanced discontinuous Galerkin methods for the shallow water equations on unstructured triangular meshes. J. Comput. Phys. 57, 19–41.
Xing, Y., Zhang, X., Shu, C.W., 2010. Positivity-preserving high order well-balanced discontinuous Galerkin methods for the shallow water equations. Adv Water Resour 33, 1476–1493.
Xu, K., 2002. A well-balanced gas-kinetic scheme for the shallow-water equations with source terms. J. Comput. Phys. 178, 533–562.
Zhang, X., Shu, C.W., 2010. On maximum-principle-satisfying high order schemes for scalar conservation laws. J. Comput. Phys. 229, 3091–3120.